



Cracking patterns of brittle hemispherical domes: an experimental study

Siwen Cao

Dept. Mechanics, Materials and Structures, Budapest University of Technology and Economics, Hungary
caosiwen.china@gmail.com

András A. Sipos

Dept. Morphology and Geometric Modeling & MTA-BME Morphodynamics Research Group, Budapest University of Technology and Economics, Hungary
siposa@eik.bme.hu, <http://orcid.org/0000-0003-0440-2165>

ABSTRACT. Crack formation in hemispherical domes is a distinguished problem in structural mechanics. The safety of cracked domes has a long track record; the evolution of the cracking pattern received less attention. Here, we report displacement-controlled loading tests of brittle hemispherical dome specimens, including the evolution of the meridional cracking pattern. The 27 investigated specimens, 20 cm in diameter, were prepared in 3D printed molds, and their material is one of the three mixtures of gypsum and cement. We find that neither the (limited) tensile strength nor the exact value of the thickness significantly affects the statistical description of the cracking pattern, i.e., the cracking phenomenon is robust. The maximal number of the meridional cracks never exceeds seven before the fragments' disintegration (collapse). We find that the size distribution of the fragments exhibits a lognormal distribution. The evolution is reflected in the load-displacement diagrams recorded in the test, too, as significant drops in the force are accompanied by an emergence of one or more new cracks, reflecting the brittle nature of the phenomenon. A simple, stochastic fragmentation model, in which a segment is fragmented at either in the middle or at the fourth point, fairly recovers the observed size distribution.

KEYWORDS. Cracking pattern; Brittle material; Hemispherical dome; Evolution; Experimental study.



Citation: Cao, S., Sipos, A.A., Cracking patterns of brittle hemispherical domes: an experimental study, *Frattura ed Integrità Strutturale*, 59 (2022) 265-310.

Received: 10.09.2021

Accepted: 03.11.2021

Published: 01.01.2022

Copyright: © 2022 This is an open access article under the terms of the CC-BY 4.0, which permits unrestricted use, distribution, and reproduction in any medium, provided the original author and source are credited.

INTRODUCTION

Transferring loads with *thin shells* is highly efficient because normal forces dominantly balance the external loads, and internal bending is marginal. With a favorable geometry (and boundary supports), internal bending mostly vanishes as long as the spatial distribution of the external loads does not vary in time [1]. The resulting material efficiency manifests in a wide range of applications, e.g., sheet metal forming, crash-worthiness test, structural design, pressure vessel



liability, and shipbuilding, to name a few [2,3]. The application of thin shells in the form of domes and other double-curved surfaces boosted the construction of large public spaces in the history of architecture. As they were built from masonry or concrete, the limited tensile strength of these materials favored compression in the shell. So, masonry or concrete shells are particularly vulnerable to internal tension and often develop cracks perpendicular to the maximal (positive) principal stress. At first sight, the stress trajectories of principal stresses seem to be an efficient tool to predict the emerging cracking pattern of the shell. Note that upon the appearance of a crack, the stress distribution, hence the direction of the stress trajectories, significantly alters. This influence of the former cracks on the formation of new ones undoubtedly influences the final cracking pattern.

Since the appearance of meridional cracks on the dome of the St. Peter's Basilica in Rome [1,4], it has become the most documented evaluation of a cracked thin shell. The debate around the origin and danger of the cracked state founded structural mechanics in its modern form [5], and it still provides a fundamental motivation to basic research [6]. Beyond this famous example, the significant number of existing structures explain that the mechanics of a cracked hemispherical dome has been widely analyzed (see [7] and the references therein). In general, a masonry dome with a sufficiently large opening angle under self-weight is subject to hoop tensile forces in their lower portion, which lead to vertical cracks appearing along the dome's meridian planes [5,8,9]. A close inspection reveals such hoop tension cracks in most of the cases. Nonetheless, a varying thickness of the shell might limit the length of these cracks. In theory, there exists a solution for a crack-free geometry [10], but it is far from practical.

The cracks of the dome open wide along with a large band and break up into fragments (called *slices*) that behave as independent pairs of semi-arches leaning on each other [7]. The dome stands as a series of arches with a standard keystone at the final extent of cracking. The collapse happens by lowering the top's weight, accompanied by significant horizontal thrusts on the bearing elements. In a monitored in-scale experiment [11,12], the classical solution to the primeval dome's thrust finds its confirmation. Some local effect often causes the initiation of cracking. E.g., Ginovart et al. [13] present the evolution of the rupture of the oval dome in Tortosa, where a failure of a roof beam led to the bending of the lantern, and the resulting asymmetric load distribution is associated with crack initiation.

Beyond static loads, chemical effects and temperature changes also play a crucial role in the cracking process. Masi et al. [8] investigate the reason and period of formation of the meridional cracks on the dome of the Pantheon in Rome. They found that concrete shrinkage, together with gravity, may have been the leading mechanical causes of the cracks in the early phases of the building's life. Qasim et al. [3] focus on fractures initiated at the remote support margins. Margin cracks can become dominant when loading forces are distributed over broad contact areas. Bartoli et al. [14] point out that the emerging cracks have a significant effect on further damage propagation and result in a complex crack pattern that fundamentally modifies the structural behavior of the dome. Instead of a hemispherical shell, the dome now behaves like four drifting half-arches. To reduce the complexity of the problem, researchers tend to focus on shallow domes, i.e., fragments of hemispherical domes [15,14], or they provide pure numerical investigations [6].

Understanding the cracking phenomenon invokes the *membrane theory of shells* [17]. It is a textbook exercise to show that the hoop stress in domes with a sufficiently high opening angle must be tensile [5]. Although the membrane theory of shells can be used to explain the principal reason behind the emerging cracking pattern, it can hardly serve as a framework for understanding the evolution of the cracks. The significant change in the stress field upon cracking mentioned above is just a partial reason. Note that the assumptions of membrane theory, especially the negligible internal bending criterion, are lost as soon as the first crack starts to propagate in the shell. Nonetheless, advanced fracture mechanics techniques provide such a modeling framework; let us mention only *variational brittle fracture*, which theory was successfully applied to predict the observed cracking pattern of the *Panthéon* in Paris [18].

Despite the long track record of the problem, the evolution of crack formation is still partially unrevealed. This paper focuses on the experimental investigation of crack development of hemispherical domes made of a homogeneous, brittle material, a gypsum-cement mixture, with limited tensile strength. After a summary of the performed experiments, the final, fragmented state and morphology development are discussed. Relation to the recorded load-displacement relationship at the top of the dome is provided. In the end, we introduce a simple stochastic model that recovers the observed size distribution of the fragments.

MATERIALS AND METHODS

Our experiments aim to reveal the evolution of the cracking pattern of complete hemispherical domes loaded with a distributed load around the top of the dome. We focus on the effect of two control parameters, the *slenderness* of the dome and the material's *tensile strength*. The $\lambda=t/R$ slenderness of the dome with radius R and thickness t



varies between $\lambda = 0.0511$ and $\lambda = 0.105$. The f_t tensile strength is varied via the gypsum/cement ratio of the material. Here we summarize the experimental setup and the execution of the testing program.

Preparation of the specimens

Hemispherical dome specimens were made of a concrete-like material without reinforcement or fiber content. During the preparation, the material was poured into a custom-made plastic mold manufactured by 3D printing. The mold consists of 3 parts, the inner mold, the outer mold, and the inner mold support (Fig.1). We aimed a constant thickness for each specimen; hence both the inner and the outer molds have a spherical surface. With $R_{out}=100\text{mm}$ radius to the outer surface, the external mold is sufficiently braced with stiffening plates. As domes with different thickness values are tested, three internal molds with different diameters were prepared. The adopted 3D printing technology used polylactic acid (PLA) filaments as a printing material [19]. After pouring, the specimens are dried at room temperature for two times 12 hours. Then the specimen is removed from the mold, and the mold is cleaned and reused for a new production cycle.

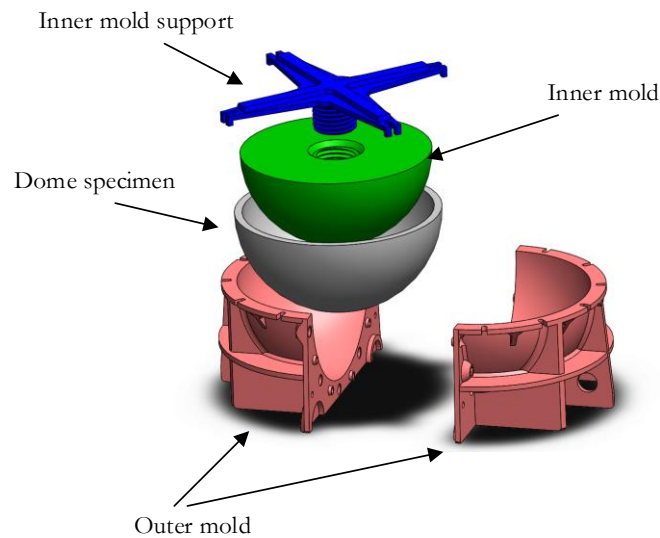


Figure 1: The 3D printed plastic mold for the preparation of the dome specimens.

The dome specimens have the following geometric properties: the outer diameter is 200 mm, the t design thicknesses are 5 mm, 7.5 mm, and 10 mm. Some of the manufactured domes are depicted in Fig.2. Note that all specimens possess an identical outer diameter. Let R_{out} denote the half of the outer diameter and R_{in} the internal radius. As the domes are with constant thickness, at any surface point $t = R_{out} - R_{in}$. As the thickness is constant, the R radius of the mid surface is simply



Figure 2: Some dome specimens after their removal from the mold.



$$R = \frac{R_{out} + R_{in}}{2} \quad (1)$$

The λ slenderness of the dome is defined via

$$\lambda = \frac{t}{R} \quad (2)$$

The relevant geometric data are summarized in Tab.1.

t (mm)	R_{out} (mm)	R_{in} (mm)	R (mm)	λ
10.0		90.0	95.00	0.105
7.5	100	92.5	96.25	0.078
5.0		95.0	97.50	0.051

Table 1: The geometry of the tested specimens.

Material

As cracks in domes are mainly tensile cracks [20], it is worthy of investigating the effect of the tensile strength on the cracking evolution. Following the ideas and practices of other researchers [21], we exploit that different ratios of cement and gypsum produce materials with different tensile strengths. After many attempts, the ratio of cement and gypsum was finally settled, as it is shown in Tab.2.

Label	(Gypsum: Cement): Water	f_t (MPa)
S2.5	(2.5: 1): 0.67	0.316
S3.0	(3.0: 1): 0.67	0.293
S3.5	(3.5: 1): 0.67	0.233

Table 2: The material parameters (by weight) and the mean of measured tensile strength.

To obtain the f_t tensile strength of the material, the widely used Brazilian Disc tests were carried out [22]. In specific, simultaneously with making the dome, cylinders with a diameter of 50 mm and a height of 50 mm were also produced using the same mixture. It means the Brazilian Disc and the dome specimens possessed identical material parameters. The strength of the material was tested on these cylinders. In order to ensure that the specimens with different material parameters have a monotonous strength relationship, a total of 3 sets of tests were done, each containing nine specimens. We found that the mean of the f_t tensile strength of the materials S2.5, S3.0, and S3.5 equals 0.316MPa, 0.293MPa, and 0.233MPa, respectively.

Labeling the specimens

We use a unique identifier for each specimen. Let the letters S, T, and L refer to *strength*, *thickness*, and *loading angle* (explained below), respectively. For instance, with these in hand, T10S2.5L30_1 means that for this dome $t=10$ mm, the ratio of gypsum and cement reads 2.5:1 (see Tab.2), and the loading angle is $\theta=30^\circ$ (see the Fig.4(b) and this letter is not varied in this study). Number 1 at the end of the label is a counter to identify the specimen uniquely.

In summary, the recommended manufacturing process for the domes (Fig.3) is as follows:

1. Scribble the vaseline to the surface of dome mold;
2. Weigh the required water, cement, and gypsum, mix them and stir for a few minutes;
3. Dump the mixture of water, cement, and gypsum into the outer mold first;
4. Assemble the inner mold: assemble, during this phase, vibrate;
5. Fasten screws while vibrating;
6. Vibrate the mold for at least 5 minutes to excrete bobbles inside the mixture;

7. Wait for 12 hours;
8. Disassemble the inside mold holder;
9. Scrape the top surface to remove extra part of the model (i.e., make the bottom surface of the model smooth);
10. Remove the inner mold;
11. Wait for 12 hours;
12. Remove the outer mold;
13. Dry it for two days;
14. Airtight the model with a plastic bag and wait for the experiment.
15. Make three Brazilian discs with the same material simultaneously (Fig.3).



Figure 3: Preparation of the specimens. Dome molds and Brazilian Discs molds with the mixture inside, after vibration.

Experimental setup

Domes were loaded vertically along their axis of symmetry. Displaced-controlled vertical pressure was applied to the upper surface of each hemispherical dome. The half-angle θ characterizes the loaded area (see Fig.4 (a)). In this investigation, the value of that angle is fixed at $\theta=30^\circ$. The pressure from the testing machine was distributed to the loaded area by a custom-made plastic spacer obtained by 3D printing. One side of the spacer is a curved surface, which can be fully attached to the dome's outer surface; the other side is a flat surface, which can be fully attached to the loading indenter (Fig.4 (b)). The spacer realizes even surface loading whole on the loaded area. At the bottom of the dome, a frictionless restraint was applied; in specific, vaseline was greased to the bottom of the dome to reduce friction.

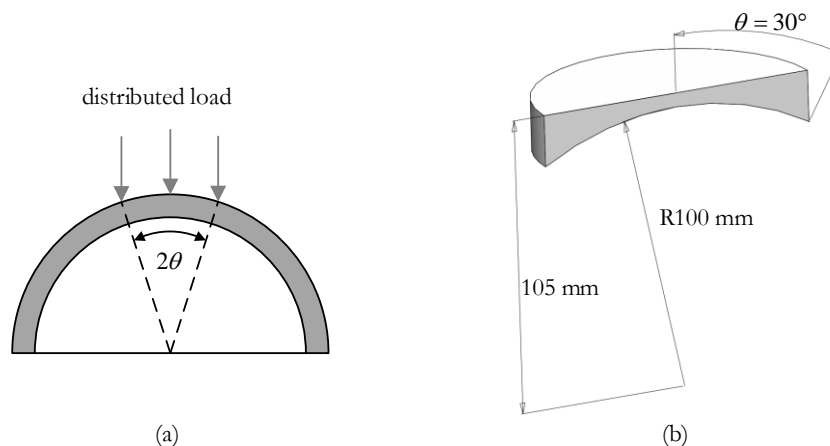


Figure 4: Loading of hemispherical specimens. (a) Half-angle θ determines the loaded area on the surface of the dome. (b) The half section schematic and size of the 3D printed plastic spacer used to distribute the load on the surface of the specimen (distances are in mm).

The experiment was performed in a Zwick/Roell Z-150 testing machine. The loading speed was 0.25 mm/min in each test. An iron plate was placed between the testing machine and the bottom of the dome. There was a positioning dial on the iron plate. The dial is used to conveniently record the relative position of the cracks (Fig.5).

Each specimen is placed on the iron plate so that it should be concentric with the dial, and the top of the dome should be aligned with the loading axis of the testing machine.



Figure 5: A specimen placed into the testing machine. Observe the plastic spacer between the specimen and the head of the testing machine.

The loading was stopped if either of two conditions was met:

1. A total collapse of the dome or complete separation of any fragment appeared due to the intersections of cracks (disintegration of the body).
2. The vertical deformation at the top of the dome exceeded 5 mm.

To obtain meaningful results, each test case was repeated three times. As we have three values for the slenderness and three material mixtures, a total of 27 specimens were investigated.

RESULTS

The geometry of the cracking pattern at the state of collapse

In the performed experiments (see Fig. 6), the maximal number N_{\max} of meridional cracks never exceeded 7; the N_{\min} minimal number was 4. The average number of cracks is $N=6.30$, with sample variance $s_N=0.87$. Two-sided student t-tests show that the observable number of the cracks is robust, i.e., influenced neither by the material quality nor the shell thickness. This latter seems slightly affecting N though so that smaller t/R results in marginally more cracks on average. (The measured data, including a photograph of the final stage, is provided as supplementary material.)

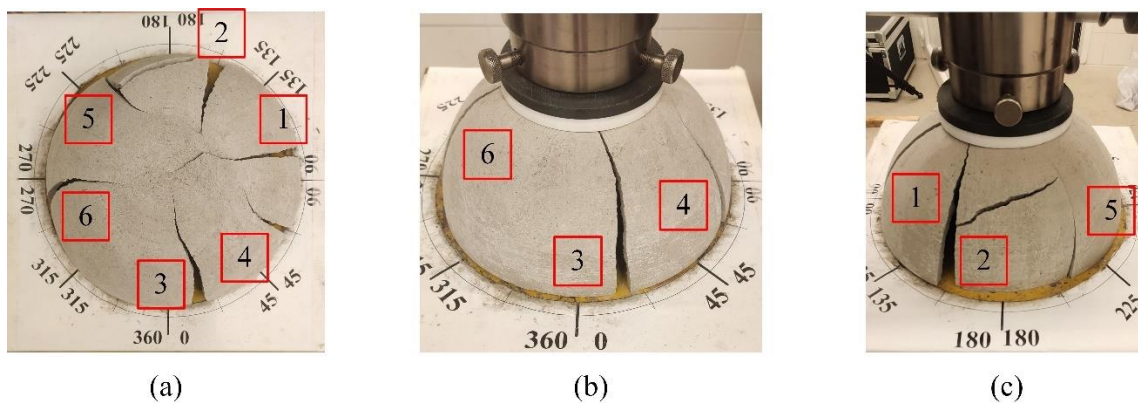


Figure 6: A cracked dome in the final stage. (a) Top view. (b) The 0 degrees angle view. (c) The 180 degrees angle view. The numbers show the order in which the crack appeared. Annexes 1 and 2 contain the photographs for each specimen.

Let Φ_{\min} denote the minimal angle between two cracks along the dome's perimeter at the final stage. Here we find, that the average reads $\Phi_{\min}=28.3^\circ$ with a sample variance of 12.9° . Two-sided student t-tests show that the material has no significant



influence on the minimal angle; however, the thickness matters: increasing t/R produces a higher minimal angle: while at $t=5$ mm the average of the minimal angle is $\Phi_{\min}=20.7^\circ$, then for $t=10$ mm it reaches $\Phi_{\min}=37.9^\circ$. Observe that in the case of a slender dome, the closest cracks have about $1/8$ of the entire perimeter.

Similarly, let Φ_{\max} denote the maximal angle between two cracks along the perimeter of the dome at the final stage. Here we find, that the average reads $\Phi_{\max}=92.9^\circ$ with a sample variance of 16.9° . Two-sided student t-tests show that neither the material nor the thickness significantly influences the maximal angle. Observe that the fragment with the maximal area without a vertical crack is close to $1/4$ of the whole perimeter.

Finally, let Φ_{avg} denote the average angle between two cracks along the dome's perimeter at the final stage. Here, in accordance with the average number of cracks, we find that the average reads $\Phi_{\text{avg}}=58.4^\circ$ with a sample variance of 9.7° . Two-sided student t-tests show that neither the material nor the thickness significantly influences the average angle. Observe that the fragment with the average area without a vertical crack is close to $1/6$ of the whole perimeter.

Given all the performed experiments, a sum of 170 fragments was produced. The distribution of the fragments concerning the angle measured on the base follows a lognormal distribution (see Fig.7) with parameters $\Phi=3.947$ and $\Phi=0.488$.

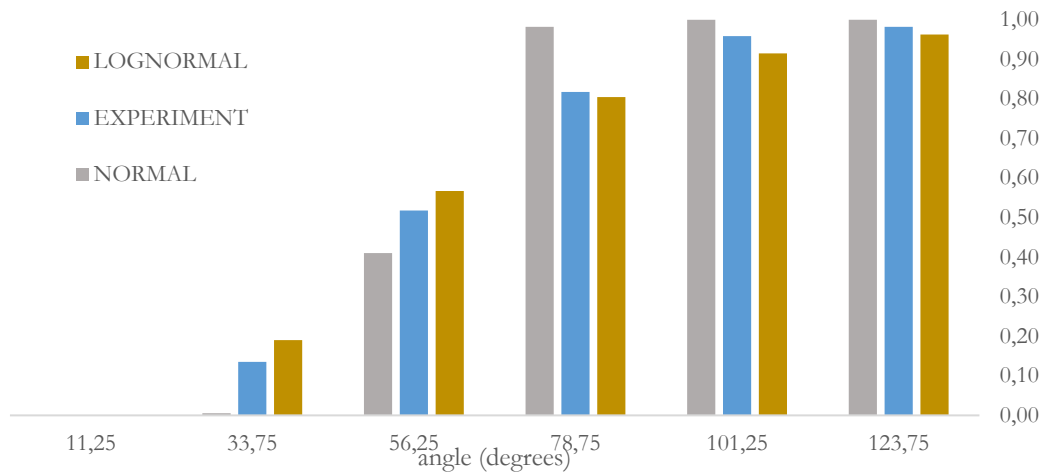


Figure 7: Cumulative distribution of the length of the fragments at the final stage. Experimental data (blue), a best-fit normal (grey), and lognormal (brown) distributions.

The evolution of the cracking pattern

Now we turn to the evolution of the cracking pattern. Observing the cracking pattern suggests that a new crack forms at the vicinity of the half point of a fragment between two cracks in many cases. However, in some other cases, the crack is close to the $1/4$ point and sometimes appears close to one of the $1/8, 3/8, 5/8, 7/8$ points of the fragment. Let L be a fixed positive integer and $0 \leq x \leq 1$ a rational number. Let $\Delta := 2^{-(L+1)}$, and we define the following sets:

$$\mathbf{A}: x \in \left\{ \frac{1}{2} \pm \Delta \right\}$$

$$\mathbf{B}: x \in \left\{ \frac{1}{4} \pm \Delta \right\} \cup \left\{ \frac{3}{4} \pm \Delta \right\}$$

$$\mathbf{C}_1: x \in \left\{ \frac{3}{8} \pm \Delta \right\} \cup \left\{ \frac{5}{8} \pm \Delta \right\}$$

$$\mathbf{C}_2: x \in \left\{ \frac{1}{8} \pm \Delta \right\} \cup \left\{ \frac{7}{8} \pm \Delta \right\}$$

$$\mathbf{D}: x \in \{0., \Delta\} \cup \{1 - \Delta ..1\} \tag{3}$$

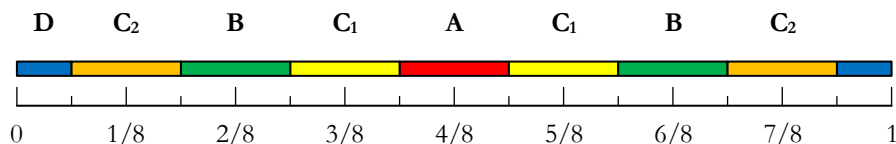


Figure 8: The sets defined by eq. (3) visualized on a line segment with unit length.

Here set **A** and **B** are in the vicinity of the middle point and a fourth of a fragment with a length of 1, respectively. Similarly, sets **C₁** and **C₂** denote the neighborhood of the eighth-points of the fragment, **C₁** is close to the middle of the fragment, **C₂** to the origin, respectively. Finally, set **D** is in the vicinity of the starting and endpoints of the fragment. The first crack appearing in the dome cannot be classified with this system (due to the rotational symmetry of the uncracked dome). The classification from the second crack can be carried out so that the position of the emerging new crack is evaluated based on the positions of the neighboring cracks. Here the angle difference between the adjacent cracks is normed to 1. In an *unscaled version*, we compute the above-defined sets for each experiment and classified the 2nd, 3rd, 4th, 5th, and 6th crack at $L=3$. The results are summarized in Tab. 3. Observe that the second crack typically appears between the midpoint and the one-fourth point of the perimeter (region **C₁**). The location of the consecutive cracks gradually moves in the direction of the middle point of the actual fragment. It is also worthy to note that in the vicinity of an existing crack, we never observe the formation of new ones (as the region **D** is empty), and the middle point itself is not that much favored, especially by cracks 2 and 3, as one would expect.

	crack2	crack3	crack4	crack5	crack6
A	18.5%	11.1%	26.9%	30.8%	18.2%
B	11.1%	40.7%	38.5%	30.8%	22.7%
C₁	44.4%	33.3%	34.6%	26.9%	59.1%
C₂	25.9%	14.8%	0.0%	11.5%	0.0%
D	0.0%	0.0%	0.0%	0.0%	0.0%

Table 3: Location-distribution of the cracks inside the fragment they appear (unscaled version). The rows of the table refer to the sets in Fig. 8. The proportions indicated in the table are calculated based on the 27 specimens. The most probable occurrence is typeset in **boldface**. Observe that cracks either appear close to the half of the fragment (sets **A** and **C₁**) or around the fourth point (set **B**).

	crack2	crack3	crack4	crack5	crack6
A	18.5%	22.2%	61.5%	65.4%	86.4%
B	11.1%	70.4%	26.9%	11.5%	4.5%
C₁	44.4%	0.0%	0.0%	0.0%	0.0%
C₂	25.9%	0.0%	0.0%	0.0%	0.0%
D	0.0%	7.4%	11.5%	23.1%	9.1%

Table 4: Location-distribution of the cracks inside the fragment they appear (scaled version). The rows of the table refer to the sets in Fig. 8. The proportions indicated in the table are calculated based on the 27 specimens. The most probable occurrence is typeset in **boldface**. Observe the tendency that cracks appearing later tend to be close to the half of the fragment (set **A**).

Note that in the previous investigation, we did not consider that the length of the fragments decreases during the fragmentation. One way to remove the effect of the length from the results above is reducing the value of L in the definition of the sets above after a fragmentation event. This evaluation is called a *scaled version*. Let L^{act} denote the value of L associated with a fragment, where the new crack forms. Nonetheless, the value of L^{act} cannot be smaller than 1 (in this case, only set **A** is meaningful). Again, starting with a single crack and $L=3$, in the experimental data, we find the following distribution



of the location of the new cracks, summarized in Tab. 4. Observe the strong tendency towards the emerging location in the middle of the fragments from crack 4. Note that this result does not contradict the findings of the unscaled version for the sixth crack: the actual length of the neighborhood of the middle point gradually decreases as the length of the fragments reduces in the process. To hit this neighborhood is more and more difficult as it shrinks towards a point. In the scaled version, we associate the neighborhood of the middle point with the $2^{-(L^{act})}$; hence, the probability of hitting this set is higher.

During the experiments, the testing machine measured the deformation, the vertical displacement of the dome crone in specific. The recorded force-displacement curves exhibit a characteristic behavior: Whenever a new crack appears, the dome deforms suddenly in the vertical direction, and the loading force drops. As the dome continuously produces cracks during the loading process, the force-deformation curve resembles a saw, as peaks appear one after another (see Fig.9). The numbers 1 to 6 in Fig. 9 represent the numbers for the consecutive cracks for the specimen T10S3.5L30_2. Between the peaks, the structure exhibits a dominantly elastic behavior reflected in a close-to-linear load-displacement curve. In about one-third of the specimens, some of the cracks appear simultaneously, i.e., two or more cracks occur at the same time. Nonetheless, this phenomenon is reflected in a more significant stress drop on the force-deformation curve.

After the appearance of several cracks (but before total collapse), elasticity seems to be lost; as the increment in the load-bearing vanishes, the structure exhibit a plastic-like behavior; however, this ductility stems from the significant movements of the fragments produced by the preceding cracking process, not the material itself. Hence, we identify two phases in the loading process (see Fig. 9): in the beginning, we observe a dominantly shell-like behavior called the *dome stage*. We come to the *arch stage* after reaching the maximal load (and the emergence of several cracks). Nonetheless, an exact definition to separate these two stages is impossible to give, as the transformation between the two is gradual.

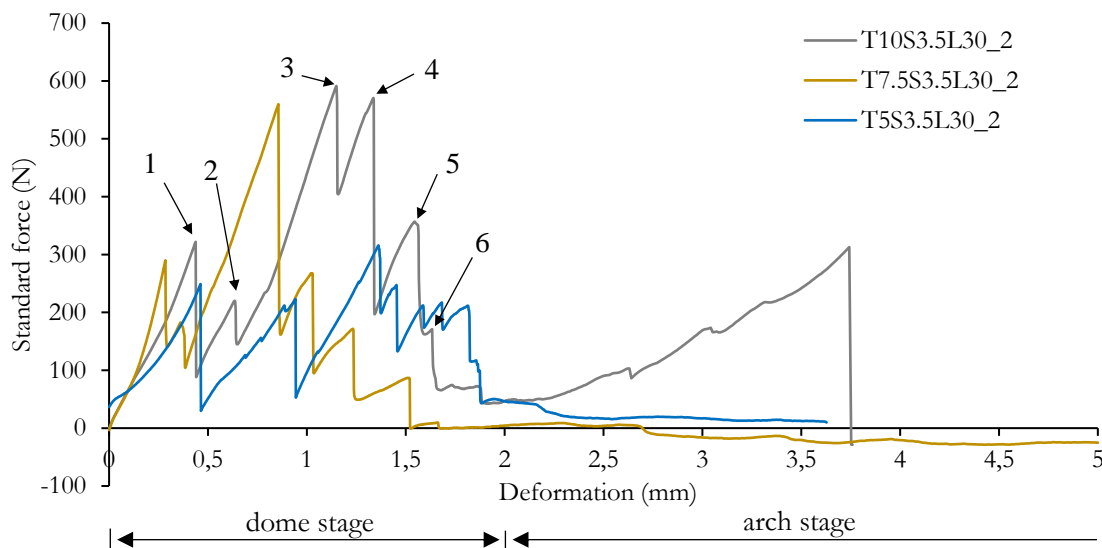


Figure 9: A load-displacement curve of three specimens. T10S3.5L30_2 (gray), T7.5S3.5L30_2 (brown), T5S3.5L30_2 (blue). The numbers show the consecutive meridional cracks of the specimen T10S3.5L30_2. Observe the linearly elastic behavior between the occurrence of two subsequent cracks and the significant drop in the force during the rapid formation of the crack.

The load-bearing capacity of the model in the arch stage is much lower than that of the dome stage. Note that the dome is a complete body; its bearing capacity depends on the t/R slenderness and the material quality; while the arch is composed of several fragments, its bearing capacity depends on the two parts, self-carrying capacity and the bottom friction. For the arch stage itself, its bearing capacity is determined by the weakest fragment.

When cracks occurred in the experiments, the minimum and maximum vertical displacement were between 0.09mm and 4.68mm. The critical vertical displacement that separates the dome and arch stages is approximately 2.0mm. The average vertical displacement at the occurrence of the first crack is about 0.55mm. A 0.37mm displacement is needed to open the second crack at a gradual increase of the load. The next cracks require respective 0.35mm, 0.29mm, 0.26mm, and 0.26mm increments in the top displacement. We see that although in some cases the appearance of two or more cracks is



simultaneous, on average, the cracks occur in well-separated intervals, and it is also meaningful that the first crack requires a bigger increment than any other.

DISCUSSION

Effect of the slenderness and the material quality

As we have seen, the fracture pattern is marginally affected by the material properties and the slenderness of the dome. This means that the geometric pattern produced by the fracture process is *robust*. Nonetheless, the maximal force is significantly differing as either the tensile strength or the slenderness of the dome is varied (Tab.5).

	S2.5	S3.0	S3.5
T10	855.9	1440.0	630.7
T7.5	725.4	720.9	778.9
T5	237.9	350.7	255.3

Table 5: Maximum loading force (N), average values.

Nonetheless, beyond the load-bearing capacity, the energy needed for the emergence of a new crack is indeed influenced by the thickness and the material quality of the specimen. In Tab. 6, the average area under the load-displacement diagram between consecutive cracks is given. Observe that the first crack requires the highest energy regardless of the thickness or the material quality in most cases. The smallest jump appears either for the fifth or the sixth crack. As the length of the cracks is, in general, equal, it shows that the phenomenon at the structural level is *quasi-brittle*, as the formation of a new crack is easier for domes with several pre-existing cracks. It is also worthy to note that the second, third and fourth crack requires more or less identical energy to form.

		crack1	crack2	crack3	crack4	crack5	crack6
T10	average	246.5	144.8	217.3	175.5	81.6	<i>50.7</i>
	variance	215.3	117.3	104.3	109.2	27.9	<i>24.1</i>
T7.5	average	197.9	62.6	87.1	88.2	<i>75.9</i>	93.6
	variance	138.3	38.5	42.0	60.2	<i>34.4</i>	87.6
T5.0	average	36.1	63.7	48.8	28.3	<i>14.9</i>	20.1
	variance	27.2	27.6	25.5	17.0	<i>12.6</i>	14.6
S2.5	average	158.7	122.2	92.6	120.0	<i>54.0</i>	55.8
	variance	177.5	125.2	65.6	123.9	<i>41.7</i>	44.2
S3.0	average	231.5	87.8	158.1	72.3	<i>61.5</i>	69.6
	variance	201.5	45.3	131.5	57.2	<i>45.8</i>	92.9
S3.5	average	90.3	61.2	102.6	76.8	50.1	27.5
	variance	101.0	34.3	80.5	65.2	38.5	19.6

Table 6: External work (N·mm) needed for the crack formation. Entries in **boldface** denote the maximal, in *italic* the minimal jumps in the strain energy.



Location of the emerging cracks

From the result of the experiments, the locations of the cracks are counted. Cracks 3 to 7 represent the order of cracks. Sort the fragment size such that 1st to 7th represents the length of the fragments from large to small. For example, the third crack (i.e., crack 3) either appears on the longer fragment (denoted to 1st) or on the smaller part (the 2nd). Similarly, crack 4 appears either on the most extended fragment (1st), the middle fragment (2nd), or the smallest fragment (3rd). The experimental distribution of the crack occurrence is given in Tab. 7. It shows that cracks tend to appear on the longer fragments, as expected.

	crack3	crack4	crack5	crack6	crack7
1st	74.07%	61.54%	70.37%	72.73%	40%
2nd	25.93%	38.46%	22.22%	18.18%	40%
3rd	-	0.00%	7.41%	9.09%	13.33%
4th	-	-	0.00%	0.00%	6.67%
5th	-	-	-	0.00%	0.00%
6th	-	-	-	-	0.00%

Table 7: The empirical probability of the next crack appearing on the fragments ordered based on their size (i.e., the 1st is the longest).

To decrease the effect of fragments number and show the tendency of a new crack occurring on bigger fragments exactly, we define M_t :

$$M_t := (L_{crack} - L_{Min}) / (L_{Max} - L_{Min}) \quad (4)$$

where, L_{crack} is the length of the fragment at which a new crack occurs, L_{Max} is the maximum length of the current fragments, and L_{Min} denotes the minimum length of current fragments. Tab. 8. shows the value of M_t for each crack, averaged for all tested specimens. M_t is not affected by the tensile strength or the thickness of the dome, and the overall mean of M_t is around 0.82.

	crack3	crack4	crack5	crack6	crack7
M_t average	0.74	0.83	0.90	0.90	0.79

Table 8: The mean of M_t for each crack.

A simple model of the cracking evolution

A simple stochastic process might be associated with the fragmentation process observed in our experiments. As in the experiments, we measured the cracks' distance in degrees, took a fragment with a length of $L=360$, and fix a threshold $0 \leq p_t \leq 1$. Let N^{act} denote the actual number of the fragments (we start with $N^{act}=1$). Let $L_1, L_2, \dots, L_{N^{act}}$ represent the length of the fragments. With a probability proportional to the size of the fragments, take a number from the set $\{1, \dots, N^{act}\}$ to select fragment i to be fragmented. Choose a random number, denoted to r , between 0 and 1. If $r < p_t$, then break fragment i into two equal parts ($L_A=L_B=L_i/2$), otherwise break it at the fourth point ($L_A=L_i/4, L_B=3L_i/4$). Increase N^{act} by one, replace L_i with L_A , and set $L_{N^{act}}=L_B$; Repeat this procedure until N^{act} reaches 6. (As the observed average number of the cracks is slightly bigger than $N=6$.)

The distribution predicted with the model at several p_t values is summarized in Fig.. Observe that between $0.5 < p_t < 0.75$, the model somewhat recovers the experimental results, implying that the stress distribution along the fragment might have at least three maxima: one at the midpoint and two others close to the fragment's end.

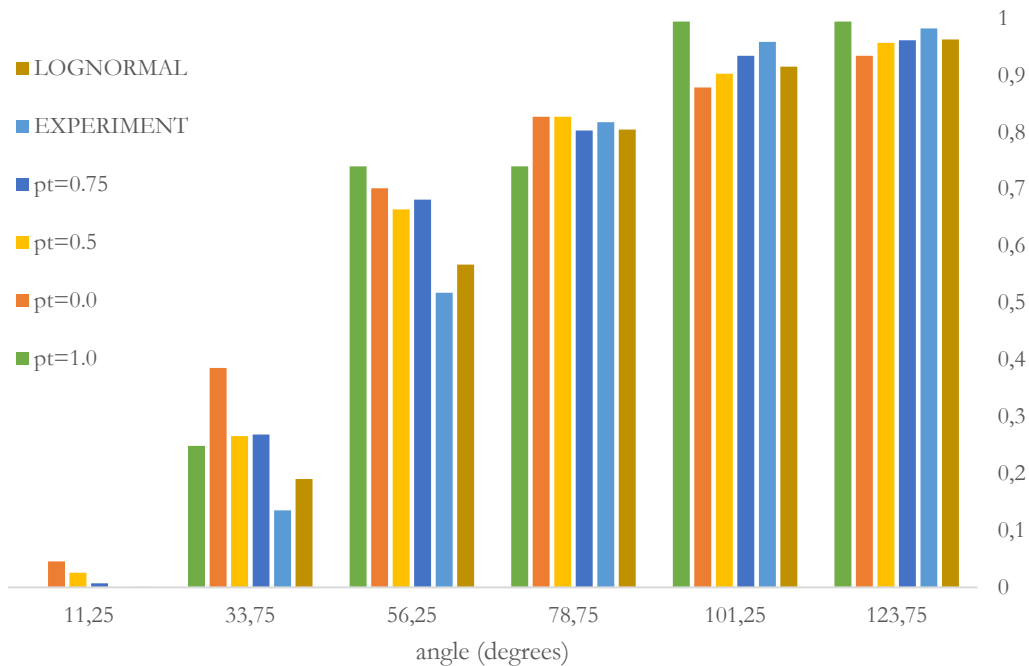


Figure 10: Cumulative distribution of the length of the fragments at the final stage. Experimental data (blue), a best-fit lognormal (brown) distribution, and the prediction of the simple stochastic model at different p_t values. Observe that both $p_t=1.0$ and $p_t=0.0$ produce a distribution far from the experimental outcome.

CONCLUSION

We carried out displacement-controlled tests on slender, hemispherical, brittle domes. Based on the experiments, we find that

1. in the practical region $0.05 \leq t/R \leq 0.10$, the thickness (i.e., the slenderness) has a marginal effect on the cracking pattern. Smaller thickness seems to produce slightly more meridional cracks on average,
2. the tensile strength of the material, as long as it is significantly smaller than the compressive strength, has a negligible effect on the cracking evolution.

These two observations support the intuition rooting in engineering practice that the cracking process of brittle domes is a *robust phenomenon* because it is mainly determined by the mid surface geometry, the supports, and the exact distribution of the external loads.

The load-displacement diagrams recorded in the tests show that a significant drop in the load accompanies cracking; however, the maximal load mainly belongs to a cracked structure with one or more cracks on the surface.

The simplistic approach about the evolution of the cracks, namely that a new crack should appear close to the midpoint between two existing cracks, seems to hold only for short fragments; the appearance of the second, third, and perhaps the fourth crack is more subtle. Regarding the size distribution of the fragments, a simple model recovers the lognormal distribution observed in the experiment. In this model, the new cracks either appear at the midpoint or the fourth point of the length-weighted, randomly selected fragment. The agreement between experimental results and model predictions shows that a simple halving procedure does not explain the observed evolution. The reason behind that might be connected to the following: before the first crack appears, the dome is in (a close-to) membrane state, i.e., the internal bending has only a marginal effect. With the propagation of the cracks, the membrane behavior is (partially) lost, the external loads are balanced with internal bending in the hoop direction. Prediction of the exact distribution of the stresses requires future work. Still, it seems that in many cases, the normal stress in the hoop direction has several maxima, presumably at the midpoint and somewhere close to the existing cracks.

Understanding the cracking evolution is not just for scientific curiosity. As many historical monuments require structural restoration, understanding the cracking evolution is highly practical: it helps to find the optimal retrofitting solution and technique [23].



ACKNOWLEDGMENTS

The research was supported by the NKFIH Grant 128584, the TKP2021-BME-NVA program, and jointly by the European Union and the Hungarian Government in the framework of Competitive Central-Hungary OP (Project ID: VEKOP-2.3.3-15-2017-00017).

REFERENCES

- [1] Heyman, J. (1998). *Structural analysis: a historical approach*, Cambridge, Cambridge University Press.
- [2] Gato, C. and Shie, Y. (2008). Numerical simulations of dynamic fracture in thin shell structures, *CMES-Computer Modeling in Engineering & Sciences*, 33(3), pp. 269-292. DOI: 10.3970/cmcs.2008.033.269.
- [3] Qasim, T., Ford, C., Bush, M.B., Hu, X., Malament, K.A. and Lawn, B.R. (2007). Margin failures in brittle dome structures: relevance to failure of dental crowns, *Journal of Biomedical Materials Research Part B: Applied Biomaterials*, 80B, pp. 78-85. DOI: 10.1002/jbm.b.30571.
- [4] Walraven, J.C. (2007). Fracture mechanics of concrete and its role in explaining structural behaviour. In A. Carpinteri, P.C. Gambarova, G. Ferro, & G.A. Plizzari (Eds.), *Fracture mechanics of concrete and concrete structures*, vol. 3: High-performance concrete, brick-masonry and environmental aspects, pp. 1265-1275. Taylor & Francis.
- [5] Heyman, J. (1995). *The stone skeleton: structural engineering of masonry architecture*, Cambridge, Cambridge University Press. DOI: 10.1017/CBO9781107050310.
- [6] Jasiński J., Raszczuk K., Kleszcz K. and Frackiewicz P. (2021) Numerical analysis of historical masonry domes: A study of St. Peter's Basilica dome, *Structures*, 31(1), pp. 80-86. DOI: 10.1016/j.istruc.2021.01.082.
- [7] Como, M. (2017). *Statics of historic masonry constructions*, 3rd ed, Berlin, Springer. DOI: 10.1007/978-3-642-30132-2.
- [8] Masi, F., Stefanou, I. and Vannucci, P. (2018). On the origin of the cracks in the dome of the Pantheon in Rome, *Engineering Failure Analysis*, 92, pp. 587–596. DOI: 10.1016/j.engfailanal.2018.06.013.
- [9] Varma, M., Ghosh, S. and Milani, G. (2018). Finite element thrust line analysis of cracked axisymmetric masonry domes reinforced with tension rings, *International Journal of Masonry Research and Innovation*, 3(1), pp. 72-87. DOI: 10.1504/IJMRI.2018.089058.
- [10] Sajtos I., Gáspár O., Sipos A.A. (2019) Geometry of the crack-free spherical masonry dome In: *Form and Force : Proceedings of the 60th Anniversary Symposium of the International Association for Shell and Spatial Structures*. ISSN 2518-6582. pp. 1-8.
- [11] Ottoni, F. (2015). Dome strengthening by encircling ties: a monitored experiment, *International Journal of Architectural Heritage*, 9(1), pp. 82-95. DOI: 10.1080/15583058.2013.793436.
- [12] Ottoni, F. and Blasi, C. (2015). Results of a 60-year monitoring system for Santa Maria del Fiore Dome in Florence, *International Journal of Architectural Heritage*, 9(1), pp. 7-24. DOI: 10.1080/15583058.2013.815291.
- [13] Ginovart, J.L.I., Costa, A., Fortuny, G., Sola-Morales, P. and Toldra, J.M. (2013). Cracking process of a oval dome in the cathedral of Tortosa, Assessment of the collapse mechanism. *Informes de la Construcción*, 65(532), pp. 509-517. DOI: 10.3989/ic.12.069.
- [14] Bartoli, G., Chiarugi, A. and Gusella, V. (1996). Monitoring systems on historic buildings: the Brunelleschi Dome, *Journal of Structural Engineering*, 122(6), pp. 663-673. DOI: 10.1061/(ASCE)0733-9445(1996)122:6(663).
- [15] Hamed, E., Bradford, M.A., Gilbert, R.I. and Chang, Z.T. (2011). Analytical model and experimental study of failure behavior of thin-walled shallow concrete domes, *Journal of Structural Engineering*, 137(1), pp. 88-99. DOI: 10.1061/(ASCE)ST.1943-541X.0000274.
- [16] Miyazaki, N. and Hagihara, S. (2015). Creep buckling of shell structures, *Mechanical Engineering Reviews*, 2(2), pp. 14-00522. DOI: 10.1299/mer.14-00522.
- [17] Timoshenko, S. and Woinowsky-Krieger, S. (1959). *Theory of Plates and Shells*. 2nd ed, New York, McGraw-Hill Book Company.
- [18] Lancioni, G. and Royer-Carfagni, G. (2009). The variational approach to fracture mechanics. A practical application to the French Panthéon in Paris, *Journal of Elasticity*, 95(1-2), pp. 1-30. DOI: 10.1007/s10659-009-9189-1.
- [19] Giordano, R. A., Wu B. M., Borland S. W., Cima L. G., Sachs E. M. and Cima M. J. (1997). Mechanical properties of dense polylactic acid structures fabricated by three-dimensional printing, *Journal of Biomaterials Science, Polymer Edition*, 8 (1), pp. 63-75 DOI: 10.1163/156856297X00588.



- [20] Quintas V. (2001). A study of the membrane state of Florence Cathedral dome, WIT Transactions on the Built Environment, 55, pp. 395-403. DOI: 10.2495/STR010381.
- [21] Bai, H., Du, W., Shou, Y., Chen, L. and Berto, F. (2021). Experimental investigation of cracking behaviors of ductile and brittle rock-like materials, Frattura ed Integrità Strutturale, 15(56), pp.16-45. DOI: 10.3221/IGF-ESIS.56.02.
- [22] Perras, M.A. and Diederichs, M.S. (2014). A review of the tensile strength of rock: concepts and testing, Geotechnical and Geological Engineering, 32(2), pp. 525-546. DOI: 10.1007/s10706-014-9732-0.
- [23] Jonbi, J. (2018). Assessment of Dome Building Damage and Repair Method. IOP Conf. Ser.: Mater. Sci. Eng. 392 062010. DOI: 10.1088/1757-899X/392/6/062010



ANNEX 1: SUPPLEMENTARY EXPERIMENT RECORD

Specimen 1 T10S2.5L30_1

Basic data				
Diameter		200 mm		Picture
Thickness		10 mm		
Dome model making date	Making	2021/6/23 10:56		
	Remove inside mold	2021/6/24 11:00		
	Remove outside mold	2021/6/24 18:00		
	Bagging	/ /		
Experiment		2021/6/25 10:00		
Ratio of raw material	Water	1680 g(for three specimens)		
	Gypsum	1800 g(for three specimens)		
	Cement	720 g(for three specimens)		
	Total(wet)	g		
	Total(dry)	g		
Experimental data				
Loading area	30 degree	Loading speed	0.25	Support <input checked="" type="checkbox"/> Free/Friction
DIC vision	--			
Experimental result				
Brazilian disk:	Diameter		50 mm	
	Length		50 mm	
	Max force		KN	
Dome	Cracks number	Position	Picture	
	1			
	2			
	3			
	4			
	5			
	6			
	7			



Specimen 2 T7.5S2.5L30_1

Basic data					
Diameter		200 mm		Picture	
Thickness		7.5 mm			
Dome model making date	Making	2021/6/23 10:56			
	Remove inside mold	2021/6/24 11:00			
	Remove outside mold	2021/6/24 18:00			
	Bagging	/ /			
	Experiment	2021/6/25 10:00			
Ratio of raw material	Water	1680 g(for three specimens)			
	Gypsum	1800 g(for three specimens)			
	Cement	720 g(for three specimens)			
	Total(wet)	g			
	Total(dry)	g			
Experimental data					
Loading area	30 degree	Loading speed	0.25	Support	Free/Friction
DIC vision	--				
Experimental result					
Brazilian disk:	Diameter		50 mm		
	Length		50 mm		
	Max force		KN		
Dome	Cracks number	Position	Picture		
	1				
	2				
	3				
	4				
	5				
	6				
	7				



Specimen 3 T5S2.5L30_1

Basic data					
Diameter		200 mm		Picture	
Thickness		5 mm			
Dome model making date	Making	2021/6/23 10:56			
	Remove inside mold	2021/6/24 11:00			
	Remove outside mold	2021/6/24 18:00			
	Bagging	/ /			
	Experiment	2021/6/25 10:00			
Ratio of raw material	Water	1680 g(for three specimens)			
	Gypsum	1800 g(for three specimens)			
	Cement	720 g(for three specimens)			
	Total(wet)	g			
	Total(dry)	g			
Experimental data					
Loading area	30 degree	Loading speed	0.25	Support	Free/Friction
DIC vision	--				
Experimental result					
Brazilian disk:	Diameter		50 mm		
	Length		50 mm		
	Max force		KN		
Dome	Cracks number	Position	Picture		
	1				
	2				
	3				
	4				
	5				
	6				
	7				
	8				
	9				

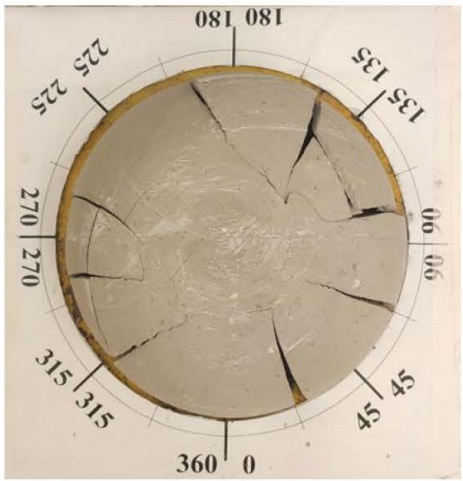
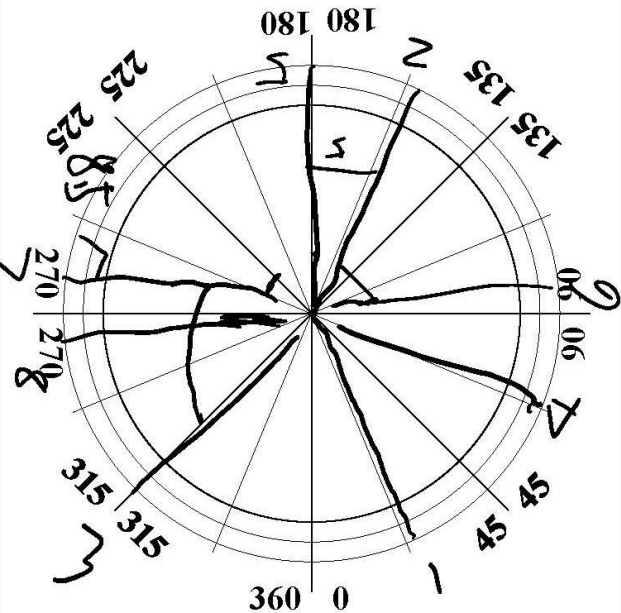


Specimen 4 T10S3.0L30_1

Basic data				
Diameter		200 mm		Picture
Thickness		10mm		
Dome model making date	Making	2021/6/25 17:30		
	Remove inside mold	2021/6/25 22:00		
	Remove outside mold	2021/6/26 6:00		
	Bagging	2021/6/27 14:30		
	Experiment	2021/6/28 10:00		
Ratio of raw material	Water	1680 g(for three specimens)		
	Gypsum	1890 g(for three specimens)		
	Cement	630 g(for three specimens)		
	Total(wet)	g		
	Total(dry)	g		
Experimental data				
Loading area		Loading speed	0.25	Support <input checked="" type="checkbox"/> Friction <input checked="" type="checkbox"/>
DIC vision	--			
Experimental result				
Brazilian disk:	Diameter		50 mm	
	Length		50 mm	
	Max force		KN	
Dome	Cracks number	Position	Picture	
	1			
	2			
	3			
	4			
	5			
	6			
	7			



Specimen 5 T7.5S3.0L30_1

Basic data				
Diameter		200 mm		Picture 
Thickness		7.5 mm		
Dome model making date	Making	2021/6/25 17:30		
	Remove inside mold	2021/6/25 22:00		
	Remove outside mold	2021/6/26 6:00		
	Bagging	2021/6/27 14:30		
	Experiment	2021/6/28 10:00		
Ratio of raw material	Water	1680 g(for three specimens)		
	Gypsum	1890 g(for three specimens)		
	Cement	630 g(for three specimens)		
	Total(wet)	g		
	Total(dry)	g		
Experimental data				
Loading area		Loading speed	0.25	Support <input checked="" type="checkbox"/> Friction <input checked="" type="checkbox"/>
DIC vision	--			
Experimental result				
Brazilian disk:	Diameter		50 mm	
	Length		50 mm	
	Max force		KN	
Dome	Cracks number	Position	Picture	
	1			
	2			
	3			
	4			
	5	lightly		
	6			
	7			
	8			
	8.5			

1 and 2 nearly together



Specimen 6 T5S3.0L30_fail

Basic data					
Diameter		200 mm		Fail	
Thickness		7.5 mm			
Dome model making date	Making		2021/6/25 17:30		
	Remove inside mold		2021/6/25 22:00		
	Remove outside mold		2021/6/26 6:00		
	Bagging		/ /		
	Experiment		/ /		
Ratio of raw material	Water		1680 g(for three specimens)		
	Gypsum		1890 g(for three specimens)		
	Cement		630 g(for three specimens)		
	Total(wet)		g		
	Total(dry)		g		
Experimental data					
Loading area		Loading speed		Support Free/Friction	
DIC vision	--				
Experimental result					
Brazilian disk:	Diameter		50 mm		
	Length		50 mm		
	Max force		KN		
Dome	Cracks number	Position			



Specimen 7 T10S3.5L30_1

Basic data					
Diameter		200 mm		Picture	
Thickness		10 mm			
Dome model making date	Making	2021/6/26 11:00			
	Remove inside mold	2021/6/26 18:30			
	Remove outside mold	2021/6/27 10:00			
	Bagging	/ /			
Experiment		2021/6/28 10:00			
Ratio of raw material	Water	1680 (for three specimens)			
	Gypsum	1960 (for three specimens)			
	Cement	560 (for three specimens)			
	Total(wet)	g			
	Total(dry)	g			
Experimental data					
Loading area		Loading speed	0.25	Support	Free Friction
DIC vision	--				
Experimental result					
Brazilian disk:	Diameter		50 mm		
	Length		50 mm		
	Max force		KN		
Dome	Cracks number	Position	Picture		
	1				
	2				
	3	lightly			
	4				
	5				
	6				
	7	together			



Specimen 8 T7.5S3.5L30_1

Basic data					
Diameter		200 mm		Picture	
Thickness		7.5 mm			
Dome model making date	Making	2021/6/26 11:00			
	Remove inside mold	2021/6/26 18:30			
	Remove outside mold	2021/6/27 10:00			
	Bagging	/ /			
	Experiment	2021/6/28 10:00			
Ratio of raw material	Water	1680 (for three specimens)			
	Gypsum	1960 (for three specimens)			
	Cement	560 (for three specimens)			
	Total(wet)	g			
	Total(dry)	g			
Experimental data					
Loading area		Loading speed	0.25	Support	Free/Friction ✓
DIC vision	--				
Experimental result					
Brazilian disk:	Diameter		50 mm		
	Length		50 mm		
	Max force		KN		
Dome	Cracks number	Position	Picture		
	1				
	2				
	3				
	4				
	5				
	6				



Specimen 9 T5S3.5L30_1

Basic data					
Diameter		200 mm		Picture	
Thickness		5 mm			
Dome model making date	Making	2021/6/26 11:00			
	Remove inside mold	2021/6/26 18:30			
	Remove outside mold	2021/6/27 10:00			
	Bagging	/ /			
	Experiment	2021/6/28 10:00			
Ratio of raw material	Water	1680 (for three specimens)			
	Gypsum	1960 (for three specimens)			
	Cement	560 (for three specimens)			
	Total(wet)	g			
	Total(dry)	g			
Experimental data					
Loading area		Loading speed	0.25	Support	Free/Friction
DIC vision	--				
Experimental result					
Brazilian disk:	Diameter		50 mm		
	Length		50 mm		
	Max force		KN		
Dome	Cracks number	Position	Picture		
	1				
	2				
	3	lightly			
	4				
	5				
	6				



Specimen 10 T10S2.5L30_2

Basic data					
Diameter		200 mm		Picture	
Thickness		10 mm			
Dome model making date	Making	2021/6/27/13:00			
	Remove inside mold	2021/6/27 20:30			
	Remove outside mold	2021/6/28 10:30			
	Bagging	2021/6/29 9:30			
	Experiment	2021/6/30 11:00			
Ratio of raw material	Water	1680 g(for three specimens)			
	Gypsum	1800 g(for three specimens)			
	Cement	720 g(for three specimens)			
	Total(wet)	g			
	Total(dry)	g			
Experimental data					
Loading area		Loading speed	0.25	Support	Free/Friction
DIC vision	--				
Experimental result					
Brazilian disk:	Diameter		50 mm		
	Length		50 mm		
	Max force		KN		
Dome	Cracks number	Position	Picture		
	1				
	2				
	3				
	4				
	5				
	6				

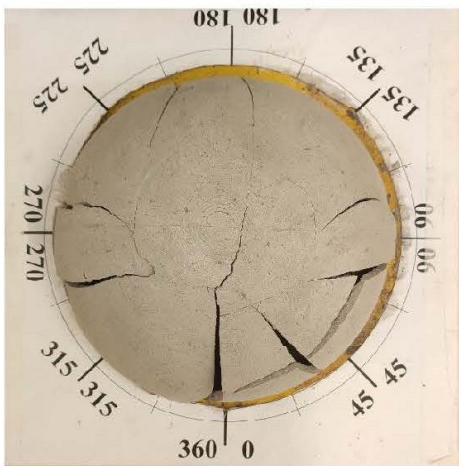
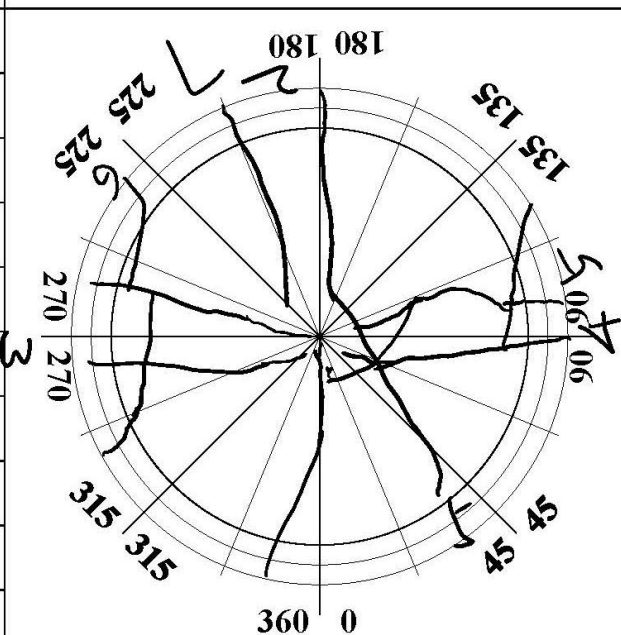


Specimen 11 T7.5S2.5L30_2

Basic data				
Diameter		200 mm		Picture
Thickness		7.5 mm		
Dome model making date	Making	2021/6/27/13:00		
	Remove inside mold	2021/6/27 20:30		
	Remove outside mold	2021/6/28 10:30		
	Bagging	2021/6/29 9:30		
	Experiment	2021/6/30 11:00		
Ratio of raw material	Water	1680 g(for three specimens)		
	Gypsum	1800 g(for three specimens)		
	Cement	720 g(for three specimens)		
	Total(wet)	g		
	Total(dry)	g		
Experimental data				
Loading area		Loading speed	0.25	Support <input checked="" type="checkbox"/> Friction <input checked="" type="checkbox"/>
DIC vision	--			
Experimental result				
Brazilian disk:	Diameter		50 mm	
	Length		50 mm	
	Max force		KN	
Dome	Cracks number	Position	Picture	
	1			
	2			
	3			
	4			
	5			
	6			
	7			
	8			



Specimen 12 T5S2.5L30_2

Basic data				
Diameter		200 mm		Picture 
Thickness		5 mm		
Dome model making date	Making	2021/6/27/13:00		
	Remove inside mold	2021/6/27 20:30		
	Remove outside mold	2021/6/28 10:30		
	Bagging	2021/6/29 9:30		
	Experiment	2021/6/30 11:00		
Ratio of raw material	Water	1680 g(for three specimens)		
	Gypsum	1800 g(for three specimens)		
	Cement	720 g(for three specimens)		
	Total(wet)	g		
	Total(dry)	g		
Experimental data				
Loading area		Loading speed	0.25	Support <input checked="" type="checkbox"/> Friction <input checked="" type="checkbox"/>
DIC vision	--			
Experimental result				
Brazilian disk:	Diameter		50 mm	
	Length		50 mm	
	Max force		KN	
Dome	Cracks number	Position	Picture	
	1			
	2			
	3			
	4			
	5			
	6			
	7			



Specimen 13 T5S3.0L30_2_add_fail

Basic data					
Diameter		200 mm		Fail	
Thickness		5 mm			
Dome model making date	Making		2021/6/28 15:30		
	Remove inside mold		2021/6/28 22:00		
	Remove outside mold		2021/6/29 9:30		
	Bagging		/ /		
	Experiment		/ /		
Ratio of raw material	Water		2240 (for four specimens)		
	Gypsum		2520 (for four specimens)		
	Cement		840 g (for four specimens)		
	Total(wet)		g		
	Total(dry)		g		
Experimental data					
Loading area		Loading speed		Support Free/Friction	
DIC vision	--				
Experimental result					
Brazilian disk:	Diameter		50 mm		
	Length		50 mm		
	Max force		KN		
Dome	Cracks number	Position			



Specimen 14 T10S3.0L30_2

Basic data					
Diameter		200 mm		Picture	
Thickness		10 mm			
Dome model making date	Making	2021/6/28 15:30			
	Remove inside mold	2021/6/28 22:00			
	Remove outside mold	2021/6/29 9:30			
	Bagging	/ /			
	Experiment	2021/6/30 11:00			
Ratio of raw material	Water	2240 (for four specimens)			
	Gypsum	2520 (for four specimens)			
	Cement	840 g (for four specimens)			
	Total(wet)	g			
	Total(dry)	g			
Experimental data					
Loading area		Loading speed	0.25	Support	Free Friction <input checked="" type="checkbox"/>
DIC vision	--				
Experimental result					
Brazilian disk:	Diameter		50 mm		
	Length		50 mm		
	Max force		KN		
Dome	Cracks number	Position	Picture		
	1				
	2				
	3	from top to bottom			
	4				
	5				
	6				
	7				



Specimen 15 T7.5S3.0L30_2

Basic data					
Diameter		200 mm		Picture	
Thickness		7.5 mm			
Dome model making date	Making	2021/6/28 15:30			
	Remove inside mold				
	Remove outside mold	2021/6/29 9:30			
	Bagging	/ /			
	Experiment	2021/6/30 11:00			
Ratio of raw material	Water	2240 (for four specimens)			
	Gypsum	2520 (for four specimens)			
	Cement	840 g (for four specimens)			
	Total(wet)	g			
	Total(dry)	g			
Experimental data					
Loading area		Loading speed	0.25	Support	Free/Friction ✓
DIC vision	--				
Experimental result					
Brazilian disk:	Diameter		50 mm		
	Length		50 mm		
	Max force		KN		
Dome	Cracks number	Position	Picture		
	1				
	2				
	3				
	4				
	5				
	6				
	7				



Specimen 16 T5S3.0L30_2

Basic data					
Diameter		200 mm		Picture	
Thickness		5 mm			
Dome model making date	Making	2021/6/28 15:30			
	Remove inside mold	2021/6/28 22:00			
	Remove outside mold	2021/6/29 9:30			
	Bagging	/ /			
	Experiment	2021/6/30 11:00			
Ratio of raw material	Water	2240 (for four specimens)			
	Gypsum	2520 (for four specimens)			
	Cement	840 g (for four specimens)			
	Total(wet)	g			
	Total(dry)	g			
Experimental data					
Loading area		Loading speed	0.25	Support	Free/Friction ✓
DIC vision	--				
Experimental result					
Brazilian disk:	Diameter		50 mm		
	Length		50 mm		
	Max force		KN		
Dome	Cracks number	Position	Picture		
	1				
	2				
	3				
	4				
	5				
	6				
	7				
	8				
	9				



Specimen 17 T10S3.5L30_2

Basic data					
Diameter		200 mm		Picture	
Thickness		10 mm			
Dome model making date	Making	2021/6/29 13:00			
	Remove inside mold	2021/6/29 22:00			
	Remove outside mold	2021/6/30 10:00			
	Bagging	2021/7/1 11:00			
	Experiment	/ /			
Ratio of raw material	Water	1680 (for three specimens)			
	Gypsum	1960 (for three specimens)			
	Cement	560 (for three specimens)			
	Total(wet)	g			
	Total(dry)	g			
Experimental data					
Loading area		Loading speed	0.25	Support	Free/Friction ✓
DIC vision	--				
Experimental result					
Brazilian disk:	Diameter		50 mm		
	Length		50 mm		
	Max force		KN		
Dome	Cracks number	Position	Picture		
	1				
	2				
	3				
	45				
	6				



Specimen 18 T7.5S3.5L30_2

Basic data				
Diameter		200 mm	Picture	
Thickness		7.5 mm		
Dome model making date	Making	2021/6/29 13:00		
	Remove inside mold	2021/6/29 22:00		
	Remove outside mold	2021/6/30 10:00		
	Bagging	2021/7/1 11:00		
	Experiment	/ /		
Ratio of raw material	Water	1680 (for three specimens)		
	Gypsum	1960 (for three specimens)		
	Cement	560 (for three specimens)		
	Total(wet)	g		
	Total(dry)	g		
Experimental data				
Loading area		Loading speed	0.25	Support <input checked="" type="checkbox"/> Free/Friction
DIC vision	--			
Experimental result				
Brazilian disk:	Diameter		50 mm	
	Length		50 mm	
	Max force		KN	
Dome	Cracks number	Position	Picture	
	1			
	2			
	3			
	4			
	5			
	6			
	7			



Specimen 19 T5S3.5L30_2

Basic data				
Diameter		200 mm		
Thickness		mm		
Dome model making date	Making	2021/6/29 13:00		
	Remove inside mold	2021/6/29 22:00		
	Remove outside mold	2021/6/30 10:00		
	Bagging	2021/7/1 11:00		
	Experiment	/ /		
Ratio of raw material	Water	1680 (for three specimens)		
	Gypsum	1960 (for three specimens)		
	Cement	560 (for three specimens)		
	Total(wet)	g		
	Total(dry)	g		
Experimental data				
Loading area		Loading speed	0.25	Support <input checked="" type="checkbox"/> Friction
DIC vision	--			
Experimental result				
Brazilian disk:	Diameter		50 mm	
	Length		50 mm	
	Max force		KN	
Dome	Cracks number	Position	Picture	
	1			
	2			
	3			
	4			
	5			
	6			
	7			
	8	from top to bottom		



Specimen 20 T10S2.5L30_3

Basic data				
Diameter		200 mm		Picture
Thickness		10 mm		
Dome model making date	Making	2021/6/30 15:30		
	Remove inside mold	2021/6/30 22:30		
	Remove outside mold	2021/7/1 11:00		
	Bagging	/ /		
	Experiment	/ /		
Ratio of raw material	Water	1680 g(for three specimens)		
	Gypsum	1800 g(for three specimens)		
	Cement	720 g(for three specimens)		
	Total(wet)	g		
	Total(dry)	g		
Experimental data				
Loading area		Loading speed	0.25	Support <input checked="" type="checkbox"/> Free/Friction
DIC vision	--			
Experimental result				
Brazilian disk:	Diameter		50 mm	
	Length		50 mm	
	Max force		KN	
Dome	Cracks number	Position	Picture	
	1			
	1.5			
	2			
	2.5			
	3			



Specimen 21 T7.5S2.5L30_3

Basic data					
Diameter		200 mm		Picture	
Thickness		7.5 mm			
Dome model making date	Making	2021/6/30 15:30			
	Remove inside mold	2021/6/30 22:30			
	Remove outside mold	2021/7/1 11:00			
	Bagging	/ /			
	Experiment	/ /			
Ratio of raw material	Water	1680 g(for three specimens)			
	Gypsum	1800 g(for three specimens)			
	Cement	720 g(for three specimens)			
	Total(wet)	g			
	Total(dry)	g			
Experimental data					
Loading area		Loading speed	0.25	Support	Friction <input checked="" type="checkbox"/>
DIC vision	--				
Experimental result					
Brazilian disk:	Diameter		50 mm		
	Length		50 mm		
	Max force		KN		
Dome	Cracks number	Position	Picture		
	12				
	3				
	4				
	5				



Specimen 22 T5S2.5L30_3

Basic data				
Diameter		200 mm	Picture	
Thickness		5 mm		
Dome model making date	Making	2021/6/30 15:30		
	Remove inside mold	2021/6/30 22:30		
	Remove outside mold	2021/7/1 11:00		
	Bagging	/ /		
	Experiment	/ /		
Ratio of raw material	Water	1680 g(for three specimens)		
	Gypsum	1800 g(for three specimens)		
	Cement	720 g(for three specimens)		
	Total(wet)	g		
	Total(dry)	g		
Experimental data				
Loading area		Loading speed	0.25	Support <input checked="" type="checkbox"/> Friction
DIC vision	--			
Experimental result				
Brazilian disk:	Diameter		50 mm	
	Length		50 mm	
	Max force		KN	
Dome	Cracks number	Position	Picture	
	1			
	2			
	3			
	4			
	5			
	6			



Specimen 23 T5S3.0L30_3_add

Basic data				
Diameter		200 mm	Picture	
Thickness		5 mm		
Dome model making date	Making	2021/7/1 13:00		
	Remove inside mold	2021/7/1 21:00		
	Remove outside mold	2021/7/2 9:30		
	Bagging	2021/7/4 11:00		
	Experiment	/ /		
Ratio of raw material	Water	2240 (for four specimens)		
	Gypsum	2520 (for four specimens)		
	Cement	840 g (for four specimens)		
	Total(wet)	g		
	Total(dry)	g		
Experimental data				
Loading area		Loading speed	0.25	Support <input checked="" type="checkbox"/> Friction <input checked="" type="checkbox"/>
DIC vision	--			
Experimental result				
Brazilian disk:	Diameter		50 mm	
	Length		50 mm	
	Max force		KN	
Dome	Cracks number	Position	Picture	
	1	0.8		
	2	1		
	3	1.38		
	4	1.4		
	5	1.9		
	6	2.4		
	7	5		



Specimen 24 T10S3.0L30_3

Basic data				
Diameter		200 mm		Picture
Thickness		10 mm		
Dome model making date	Making	2021/7/1 13:00		
	Remove inside mold	2021/7/1 21:00		
	Remove outside mold	2021/7/2 9:30		
	Bagging	2021/7/4 11:00		
	Experiment	2020 / 7 / 17:10		
Ratio of raw material	Water	2240 (for four specimens)		
	Gypsum	2520 (for four specimens)		
	Cement	840 g (for four specimens)		
	Total(wet)	g		
	Total(dry)	g		
Experimental data				
Loading area		Loading speed	0.25	Support <input checked="" type="checkbox"/> Free/Friction
DIC vision	--			
Experimental result				
Brazilian disk:	Diameter		50 mm	
	Length		50 mm	
	Max force		KN	
Dome	Cracks number	Position	Picture	
	1	1		
	2	1.2		
	3456	1.8		
		.		



Specimen 25 T7.5S3.0L30_3

Basic data					
Diameter		200 mm		Picture	
Thickness		7.5 mm			
Dome model making date	Making	2021/7/1 13:00			
	Remove inside mold	2021/7/1 21:00			
	Remove outside mold	2021/7/2 9:30			
	Bagging	2021/7/4 11:00			
	Experiment	/ / 10:35			
Ratio of raw material	Water	2240 (for four specimens)			
	Gypsum	2520 (for four specimens)			
	Cement	840 g (for four specimens)			
	Total(wet)	g			
	Total(dry)	g			
Experimental data					
Loading area		Loading speed	0.25	Support	Free/Friction ✓
DIC vision	--				
Experimental result					
Brazilian disk:	Diameter		50 mm		
	Length		50 mm		
	Max force		KN		
Dome	Cracks number	Position	Picture		
	1	0.8			
	2	1			
	3	1.2			
	4	1.4			
	5	1.5			
	6	1.8			



Specimen 26 T5S3.0L30_3

Basic data				
Diameter		200 mm	Picture	
Thickness		5 mm		
Dome model making date	Making	2021/7/1 13:00		
	Remove inside mold	2021/7/1 21:00		
	Remove outside mold	2021/7/2 9:30		
	Bagging	2021/7/4 11:00		
	Experiment	/ / / / : : /		
Ratio of raw material	Water	2240 (for four specimens)		
	Gypsum	2520 (for four specimens)		
	Cement	840 g (for four specimens)		
	Total(wet)	g		
	Total(dry)	g		
Experimental data				
Loading area		Loading speed	0.2	Support <input checked="" type="checkbox"/> Free Friction <input checked="" type="checkbox"/>
DIC vision	--			
Experimental result				
Brazilian disk:	Diameter		50 mm	
	Length		50 mm	
	Max force		KN	
Dome	Cracks number	Position	Picture	
	1	0.6		
	2	1.4		
	3	1.7		
	4	2.2		
	5	2.28		
	6	2.35		



Specimen 27 T10S3.5L30_3

Basic data					
Diameter		200 mm		Picture	
Thickness		10 mm			
Dome model making date	Making	2021/7/3 14:00			
	Remove inside mold	2021/7/3 23:00			
	Remove outside mold	2021/7/4 11:00			
	Bagging	/ /			
	Experiment	/ /			
Ratio of raw material	Water	1680 (for three specimens)			
	Gypsum	1960 (for three specimens)			
	Cement	560 (for three specimens)			
	Total(wet)	g			
	Total(dry)	g			
Experimental data					
Loading area		Loading speed	0.25	Support	Free/Friction
DIC vision	--				
Experimental result					
Brazilian disk:	Diameter		50 mm		
	Length		50 mm		
	Max force		KN		
Dome	Cracks number	Position	Picture		
	1	0.5			
	2	0.8			
	3	1.2			
	4	1.3			
	5	1.6			
	6	1.8			
	7	1.8			



Specimen 28 T7.5S3.5L30_3

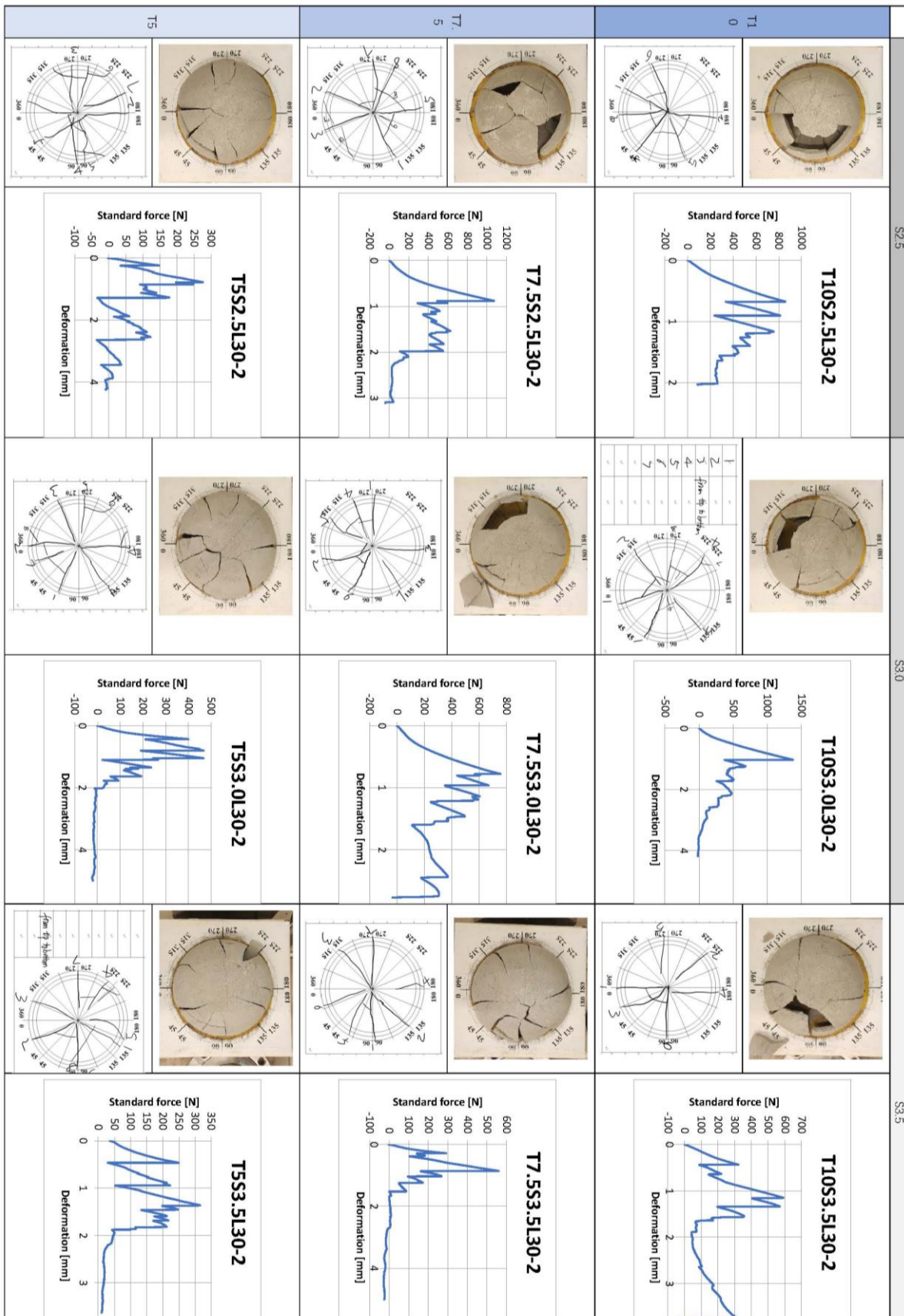
Basic data				
Diameter		200 mm		Picture
Thickness		7.5 mm		
Dome model making date	Making	2021/7/3 14:00		
	Remove inside mold	2021/7/3 23:00		
	Remove outside mold	2021/7/4 11:00		
	Bagging	/ / 11:47		
Ratio of raw material	Experiment	/ /		
	Water	1680 (for three specimens)		
	Gypsum	1960 (for three specimens)		
	Cement	560 (for three specimens)		
	Total(wet)	g		
Total(dry)	g			
Experimental data				
Loading area		Loading speed	0.25	Support <input checked="" type="checkbox"/> Free/Friction
DIC vision	--			
Experimental result				
Brazilian disk:	Diameter		50 mm	
	Length		50 mm	
	Max force		KN	
Dome	Cracks number	Position	Picture	
	1	0.6		
	2	0.7		
	3	0.8		
	4	1.4		
	5	1.6		



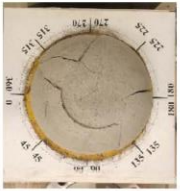
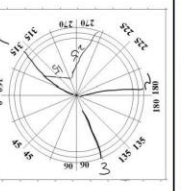
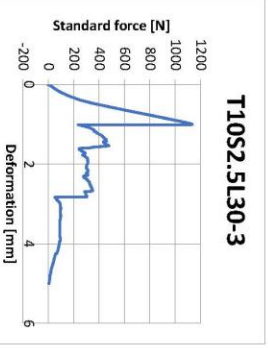
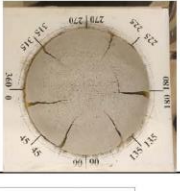
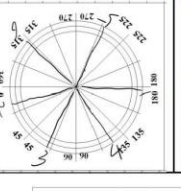
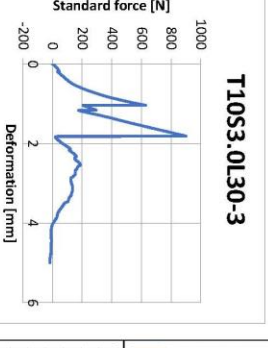
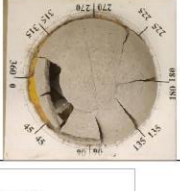
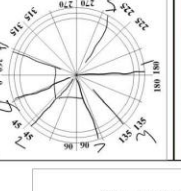
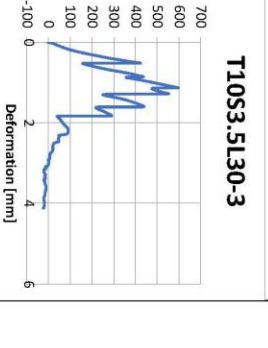
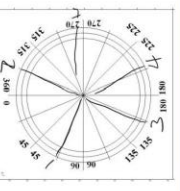
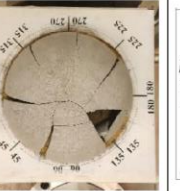
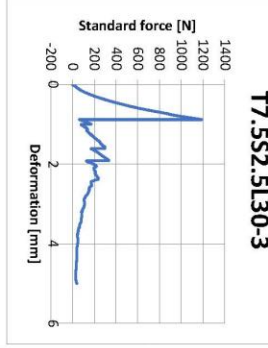
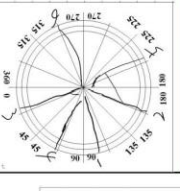
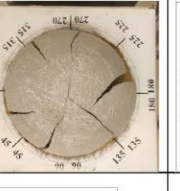
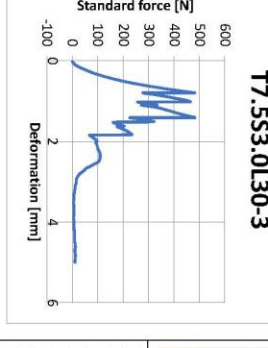
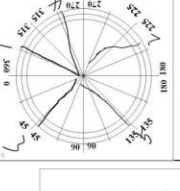
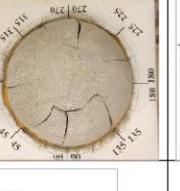
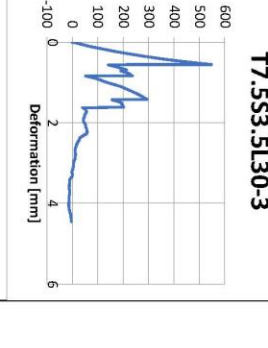
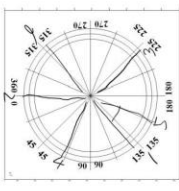
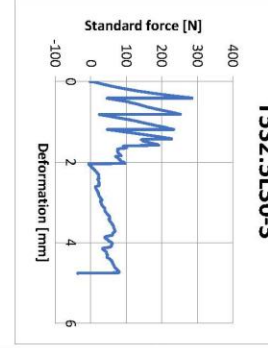
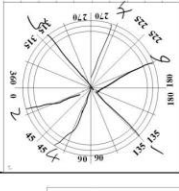
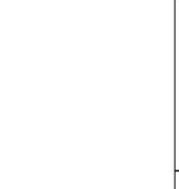
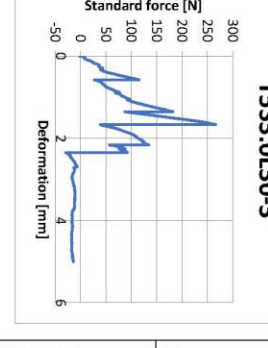
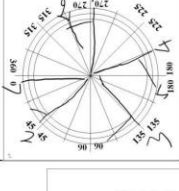
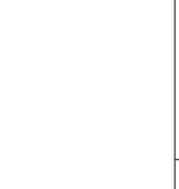
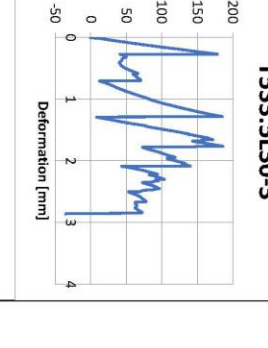
Specimen 29 T5S3.5L30_3

Basic data				
Diameter		200 mm		
Thickness		5 mm		
Dome model making date	Making	2021/7/3 14:00		
	Remove inside mold	2021/7/3 23:00		
	Remove outside mold	2021/7/4 11:00		
	Bagging	/ / 12:09		
	Experiment	/ /		
Ratio of raw material	Water	1680 (for three specimens)		
	Gypsum	1960 (for three specimens)		
	Cement	560 (for three specimens)		
	Total(wet)	g		
	Total(dry)	g		
Experimental data				
Loading area		Loading speed	0.25	Support <input checked="" type="checkbox"/> Friction <input checked="" type="checkbox"/>
DIC vision	--			
Experimental result				
Brazilian disk:	Diameter		50 mm	
	Length		50 mm	
	Max force		KN	
Dome	Cracks number	Position	Picture	
	1	0.2		
	2	0.7		
	3,4	1.3		
	5	1.8		
	6	1.9		
	7	2.1		

ANNEX 2: SUPPLEMENTARY LOAD-DISPLACEMENT DIAGRAMS





	S2.5		S3.0		S3.5	
T10	 	 T10S2.5L30-3	 	 T10S3.0L30-3	 	 T10S3.5L30-3
T7.5	 	 T7.5S2.5L30-3	 	 T7.5S3.0L30-3	 	 T7.5S3.5L30-3
T5	 	 T5S2.5L30-3	 	 T5S3.0L30-3	 	 T5S3.5L30-3

